Identification and Small-Signal Analysis of Interaction Modes in VSC MTDC Systems

Beerten, j.; d'Arco, S.; Suul. J.A

Identification and Small-Signal Analysis of Interaction Modes in VSC MTDC Systems

Jef Beerten, *Member, IEEE,* Salvatore D'Arco, Jon Are Suul, *Member, IEEE*

***Abstract*—In this paper, a methodology is presented to identify and analyse interaction modes between converters in Voltage Source Converter Multi-Terminal High Voltage Direct Current (VSC MTDC) systems. The absence of a substantial level of energy stored in such power electronics based systems results in fast system dynamics, governed by electromagnetic phenomena. Moreover, interactions between components are largely influenced by the control parameters and in general, an a-priori identification of interaction modes based on associated time constants is less straight-forward than in AC systems. Furthermore, the extent to which converters interact not only depends on the controller parameters, but is also influenced by the physical characteristics of the HVDC system. The methodology introduced in this paper is based on aggregated participation factors to distinguish between local modes, primarily associated with one terminal, and interaction modes involving multiple terminals. To illustrate the proposed methodology, the influence of droop control parameters, as well as DC breaker inductors, on the system dynamics and the participation of the terminals are investigated for a three-terminal MTDC system.**

***Index Terms*—HVDC transmission, Multi-terminal HVDC, Small-signal dynamics, Converter interactions.**

I. Introduction

In recent years, the power industry is showing an increasing interest in High Voltage Direct Current (HVDC) transmission based on Voltage Source Converters (VSC) in a multi-terminal (MTDC) or even meshed grid configuration to connect offshore wind farms [1]. Although the technology has been in operation in point-to-point links, the operation of several converters in an MTDC system poses a number of technical challenges. Since larger HVDC grids will most likely be multi-vendor systems with potentially different converter technologies operating in the same grid, a critical aspect concerns the interoperability and the prediction of possible adverse interactions between the terminal. In AC systems, the fundamentals of adverse interactions between generators are well understood and a small-signal stability analysis is typically used to distinguish between local modes and slower interarea modes [2]. Furthermore, the large generators' inertia provides a physical basis for a classification of stability phenomena [3]. In an HVDC grid, however, the distinction is less obvious: the time constants governing the system response are much smaller as they are determined by the capacitive discharge of the cables and converter DC capacitors. Consequentially, the controller settings can have a significant impact on the nature of the interactions, which are not necessarily limited to the converters, but can also involve other system components.

Since most operating schemes until today are two-terminal systems with a centralised DC voltage control, the stability analysis has mainly been limited to the interaction with the AC system. For the analysis of local interactions with the power system, the converter can usually be simplified as a controllable voltage source, whilst retaining a detailed representation of the converter controllers [4], [5]. Moreover, a reduced model of the AC system, namely a voltage source with a complex impedance based on the short-circuit ratio (SCR) at the Point of Common Coupling (PCC), is in general sufficient to study the stability of the controller [6], [7]. For such AC system interaction studies, the DC system itself can be simplified by only retaining the overall voltage dynamics in the system [5].

The expected advent of multi-terminal systems triggered the development of a new breed of linearised models to study control interactions involving several converters [8]–[13]. In [8], the stability of voltage droop controlled converters in a DC system was discussed using singular value decomposition of a linearised model of the converter controllers and the DC system. However, the focus was on the voltage droop gain and possible adverse interactions with other control loops were not included. Furthermore, the DC grid dynamics were accounted for by lumped impedance models. In [9] and [11], a small-signal stability model was developed, but by straightforwardly extending the operation principles of two-terminal schemes, the models did not account for a distributed voltage control based on a droop control action. Moreover, none of the studies considers the possible adverse influence of the DC breakers' inductors on the DC voltage control stability. Recently, these aspects were taken into account in [14].

This paper aims at introducing a systematic identification of interaction modes in a VSC MTDC system by analysing the participation of the different system components in these modes. The paper is organised as follows: Section II introduces the mathematical modelling approach. Section III puts forward the identification method. Section IV discusses the simulation results in a three-terminal system, both under constant voltage and droop control. Furthermore, the influence of system parameters on the nature of the interactions are investigated.

Jef Beerten is funded by a postdoctoral research grant from the Research Foundation – Flanders (FWO). The work of SINTEF Energy Research in this paper was supported by the project "Protection and Fault Handling in Offshore HVDC Grids – ProOfGrids," financed by the Norwegian Research Council together with industry partners EDF, National Grid, Siemens, Statkraft, Statnett, Statoil and NVE.

Jef Beerten is with the Department of Electrical Engineering (ESAT), Division ELECTA & EnergyVille, University of Leuven (KU Leuven), Kasteelpark Arenberg 10, bus 2445, 3001 Leuven-Heverlee, Belgium and also with the Department of Electric Power Engineering, Norwegian University of Science and Technology (NTNU), 7495 Trondheim, Norway (e-mail: jef.beerten@esat.kuleuven.be). Salvatore D'Arco is with SINTEF Energy Research, 7465 Trondheim, Norway (e-mail: salvatore.darco@sintef.no). Jon Are Suul is with the Department of Electric Power Engineering, NTNU and also with SINTEF Energy Research (e-mail: jon.a.suul@sintef.no).

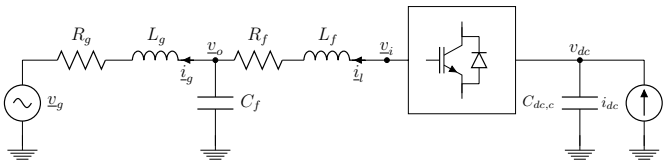

Figure 1. Converter state-space model.

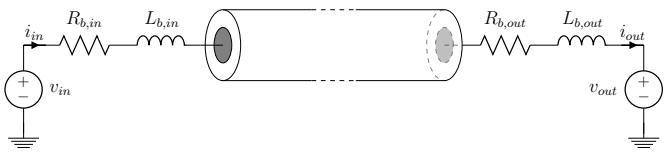

Figure 2. Cable terminated by inductors.

II. Mathematical modelling

To maintain the flexibility to model systems with arbitrary topologies, the different components in the HVDC system (cables and converters) are first derived as independent linear time-invariant subsystems in a state-space format. The dynamics for the entire system are thereafter derived by assembling the subsystems. Each subsystem is modelled as a linearised system

$$\dot{\boldsymbol{x}} = \mathsf{A}\boldsymbol{x} + \mathsf{B}\boldsymbol{u}\ ;\ \boldsymbol{x}(0) = \boldsymbol{x_0}, \tag{1}$$

with $\boldsymbol{x} \in \mathbb{R}^n$ the state vector, $\boldsymbol{u} \in \mathbb{R}^m$ the input vector and $\mathsf{A} \in \mathbb{R}^{n\times n}$, $\mathsf{B} \in \mathbb{R}^{n\times m}$ the known coefficient matrices that can be a function of the steady-state linearisation around $\boldsymbol{x_0} \in \mathbb{R}^n$. Further details on the modular modelling procedures are found in [15], [16].

A. Converter terminal modelling

The converter and its control loops can be derived in the form of (1). The converter model used in this study is based on the model described in [17], an averaged two-level converter model, including filter bus dynamics. The connection to the grid is taken into account using a complex impedance, which represents the combination of the transformer and the grid Thevenin impedance. A phase-locked loop (PLL) is used to synchronise the dq reference frame to the voltage at the filter bus. Additional control loops include decoupled inner current controllers, active power or DC voltage control. Both can be extended with an outer droop control loop, resulting in two different implementations. Further dynamics are related to the low pass filtering of the measurements of the current, DC voltage and active power. Outer control loops for the reactive power have been left out of the study.

Fig. 1 indicates how the converter is modelled separately as a building block for the state-space representation. The current at the DC side is considered as an input to the model, as are the AC voltage source and the references for the controllers. The result is an 18th-order model, in which the converter DC voltage appears as the state variable that needs to be linked with the other components in the system. The steady-state conditions can be calculated independently for this building block by assuming a certain input vector and are used to linearise the system around the operating point.

B. Cable modelling

The HVDC cables are modelled with a state-space representation based on cascaded pi elements with parallel series branches as in [18]. The parallel branches of the pi elements, calculated using vector fitting [19], allow to incorporate the frequency dependence of the series cable parameters R and L. Fig. 2 illustrates how the cable is modelled as an independent state-space building block, terminated with inductors L_b to represent the current limiting reactors of DC breakers and its corresponding resistance R_b. Fig. 3 shows the corresponding state-space model, while the expressions in the appendix indicate how the cable model from [18] is extended to account for the presence of the DC breakers.

C. Aggregation of subsystem models

With all different subsystems described in the form of (1), a state-space model of the entire system is assembled.

A first step is to determine the steady state condition for the entire system in order to define the operating point for each subsystem. Hence, a steady-state solution for the DC system is required, taking into account the DC system losses. As a result, one obtains the state-space models of the different components. For component i

$$\dot{\boldsymbol{x}}_{\boldsymbol{i}} = \mathsf{A}_\mathsf{i}\boldsymbol{x}_{\boldsymbol{i}} + \mathsf{B}_\mathsf{i}\boldsymbol{u}_{\boldsymbol{i}}, \tag{2}$$

with $\boldsymbol{x_i} \in \mathbb{R}^{n_i}$ the component's state variables, $\boldsymbol{u_i} \in \mathbb{R}^{m_i}$ the input variables, $\mathsf{A}_\mathsf{i} \in \mathbb{R}^{n_i\times n_i}$ their component's state-space matrix and $\mathsf{B}_\mathsf{i} \in \mathbb{R}^{n_i\times m_i}$ the input matrix.

The overall system matrix A_t can be assembled by accounting for the "interface variables", i.e. state variables of subsystems that are input variables for other subsystems. More specifically, these are the DC currents at the cable ends and the converter DC voltages. The state-space model for a system of p components can be written as

$$\dot{\boldsymbol{x}}_{\boldsymbol{t}} = \mathsf{A}_\mathsf{t}\boldsymbol{x}_{\boldsymbol{t}} + \mathsf{B}_\mathsf{t}\boldsymbol{u}_{\boldsymbol{t}}, \tag{3}$$

with

$$\boldsymbol{x_t} = \begin{bmatrix}\boldsymbol{x_1} & \dots & \boldsymbol{x_p}\end{bmatrix}^T, \tag{4}$$

$$\boldsymbol{u_t} = \begin{bmatrix}\boldsymbol{u_1^r} & \dots & \boldsymbol{u_p^r}\end{bmatrix}^T. \tag{5}$$

assuming no overlapping states in the modelling of the components, $\boldsymbol{x_t} \in \mathbb{R}^{n_t}$ with $n_t = \sum_{i=1}^{p} n_i$. The resulting input vector $\boldsymbol{u_t} \in \mathbb{R}^{m_t}$ only consists of reduced versions $\boldsymbol{u_i^r} \in \mathbb{R}^{m_i^r}$ of the converter input vectors, since the DC currents, which are inputs to the converter model (Fig. 1), are state variables related to the cable subsystems. Similarly, the DC voltages are state variables related to the converters' subsystems and the input vector for the cable j is eliminated by substituting the corresponding columns of B_j in A_t.

III. Component interaction identification

The interactions between the different component are studied with the system model from (3)–(5). As a first step, a

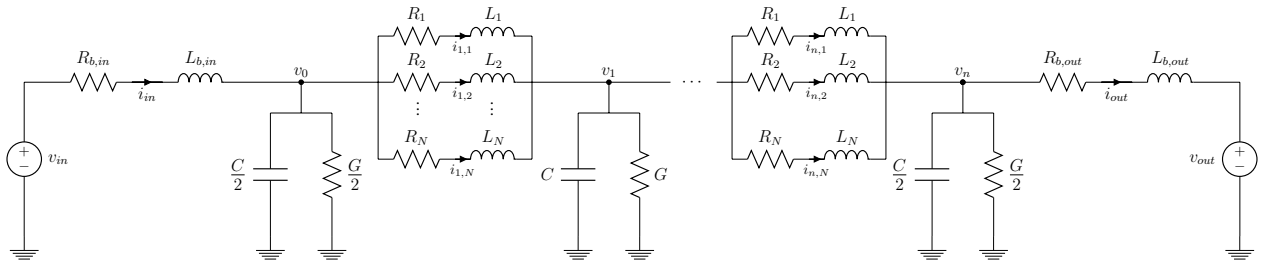

Figure 3. Cable state-space model.

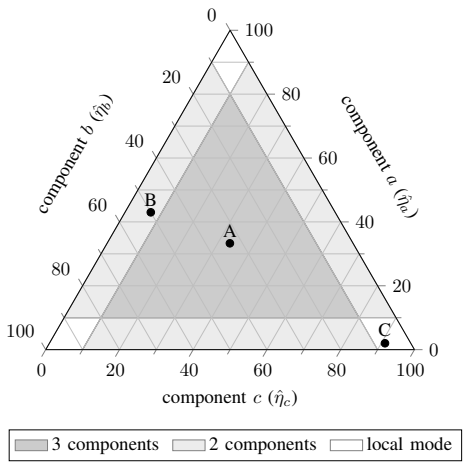

Figure 4. Component interaction representation.

criterion is defined to classify the modes as either local or interaction modes, where interaction modes are defined as modes in which at least two converters participate. These modes can be identified on the basis of participation factors. Let p_{ki} denote the participation factor of state variable x_k in mode i, defined as [2]

$$p_{ki} = \phi_{ki}\psi_{ik}, \tag{6}$$

with ϕ_{ki} the k-th entry of the right eigenvector $\boldsymbol{\phi_i} \in \mathbb{R}^{\boldsymbol{n_t}}$ and ψ_{ik} the k-th entry of the left eigenvector $\boldsymbol{\psi_i} \in \mathbb{R}^{\boldsymbol{n_t}}$. Let $\boldsymbol{p_i} \in \mathbb{R}^{n_t}$ be the vector with the participation factors for all system states, and associated with mode i. Similarly, $\boldsymbol{p_{\alpha,i}} \in \mathbb{R}^{n_\alpha}$ is the vector for all states of subsystem α.

We now define the parameter $\eta_{\alpha i}$ as a measure for the overall participation for each subsystem α in mode i such that

$$\eta_{\alpha i} = \frac{\|\boldsymbol{p_{\alpha,i}}\|}{\|\boldsymbol{p_i}\|}, \tag{7}$$

with $\|\cdot\|$ denoting the L_1-norm. $\eta_{\alpha i}$ is thus a measure for the degree to which the component α participates in mode i. Defining a threshold χ, we define an interaction mode i between two components a and b as a mode for which both $\eta_{ai} > \chi$ and $\eta_{bi} > \chi$, resulting in a subset of interaction modes $\mathcal{S}^{a,b}$.

The definition can be extended to more components. When particularly interactions between a subset of components $\mathcal{I}$ are of interest, a set of interaction modes $\mathcal{S}$ can be defined as

$$\mathcal{S} = \{i \mid \eta_{\alpha i} > \chi,\, \forall \alpha \in \mathcal{I}\}, \tag{8}$$

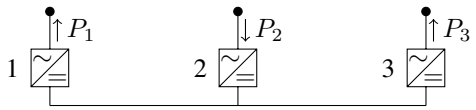

Figure 5. Three-terminal VSC MTDC system configuration.

Analogously, a subset of interaction modes $\mathcal{S}^{\mathcal{A}}$ is defined, consisting of modes in which some, but not all components in $\mathcal{I}$ are involved. With $\mathcal{I}^{\mathcal{A}}$ denoting the subset of components from $\mathcal{I}$

$$\mathcal{S}^{\mathcal{A}} = \left\{i \mid \eta_{\alpha i} > \chi,\, \forall \alpha \in \mathcal{I}^{\mathcal{A}} \text{ and } \eta_{\beta i} \leq \chi,\, \forall \beta \in \mathcal{I}^{\mathcal{B}}\right\}, \tag{9}$$

with the set of components $\mathcal{I}^{\mathcal{B}}$ defined as $\mathcal{I}^{\mathcal{B}} = \mathcal{I} \setminus \mathcal{I}^{\mathcal{A}}$.

The relative participation of components α with respect to the subset $\mathcal{I}$ can be defined as

$$\hat{\eta}_{\alpha i} = \frac{\eta_{\alpha i}}{\sum\limits_{x \in \mathcal{I}} \eta_{xi}}. \tag{10}$$

As a generic example, in case where a subset of three components a, b and c is considered, a so-called ternary diagram can be used to represent the relative participation of each of the three components. Fig. 4 offers an example with the threshold χ equal to 10%. The location of the modes in this diagram determines to relative participation of the three components. Mode A is a mode in which the three components participate about equally. The area marked in dark gray contains all the modes in which the three converters participate. Similarly, mode B has about equal participation from components a, and b, whilst component c does not participate in the mode. Mode C on the other hand, is a 'local' mode associated with component c, but not with components a and b. Attention needs to be paid to the fact that the position in the ternary diagram only indicates the relative contributions of the three components ($\hat{\eta}_{\alpha i}$). In other words, when there are more than three components in the system and when, for a given mode i, $\eta_{\Sigma_{\mathcal{I}} i} < 1$ with $\eta_{\Sigma_{\mathcal{I}} i} = \sum_{x \in \mathcal{I}} \eta_{xi}$, the position of the mode in the diagram only provides information about the relative contributions of the three components compared to each other. The contribution of the other components in the network will be visualised in the ternary diagram by grouping these remaining components and changing the luminance accordingly. Another consequence is that the shaded areas cannot directly be applied for the modes i for which $\sum_{x \in \mathcal{I}} \hat{\eta}_{xi} < 1$, as the absolute relation $\eta_{\alpha_i} > \chi$ turns into a relative one as a result of the scaling, or $\hat{\eta}_{\alpha_i} > \hat{\chi}$ with $\hat{\chi} = \chi / \eta_{\Sigma_{\mathcal{I}} i}$. Consequentially,

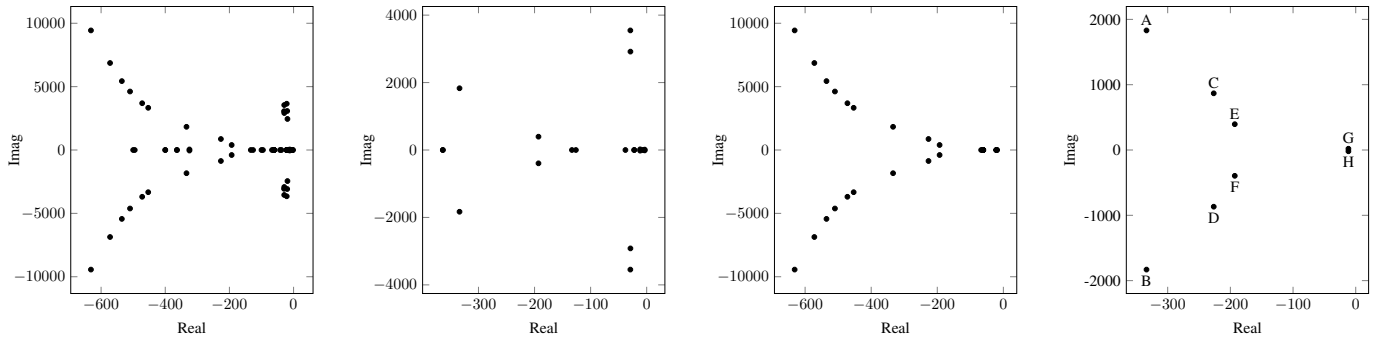

(a) Eigenvalues $\mathsf{A_t}$ (system) (b) Modes converter 1 ($\eta_1 > 5\%$) (c) Cable modes ($\eta_{1\text{-}2}+\eta_{2\text{-}3} > 50\%$) (d) Converter interaction modes ($\eta_{co} > 5\%$ for at least 2 converters)

Figure 6. Pole location of the system matrix $\mathsf{A_t}$, modes related to converter 1, cable modes, converter interaction modes – power control on converters 1 and 3, voltage control on converter 2.

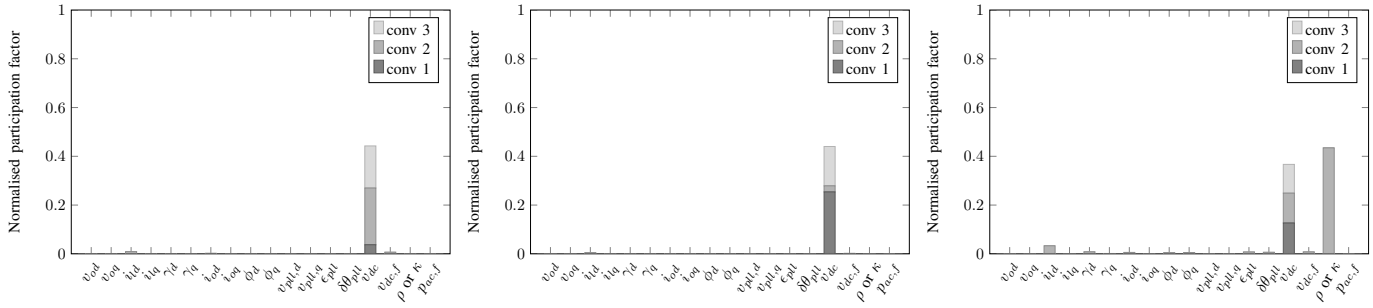

(a) Participation in modes C,D (b) Participation in modes E,F (c) Participation in modes G,H

Figure 7. Participation in selected interaction modes – voltage control in converter 2, power control in converters 1 and 3.

the area indicating interactions between the three components shrinks accordingly with lower values of $\eta_{\Sigma_{\mathcal{I}}i}$.

IV. Converter interactions in MTDC systems

The identification from the previous section is applied to a three-terminal MTDC system. The configuration, shown in Fig. 5, is based on a symmetrical monopolar system with voltage ratings of $\pm$320 kV. The three converters and the cables have a rated power of 1000 MW. The cable between converters 1 and 2 is 300 km long, whereas the cable between converters 2 and 3 is 150 km long. The cables have been modelled using the model from [18], with 5 parallel branches and 5 parallel sections. Cable data are based on the model presented in [20]. The AC side parameters of the two-level converter configuration have been taken from [21]. The inner current controller has been tuned to obtain a critically damped system with an equivalent time constant of 2.5 ms.

A. Centralised voltage control

In a first case study, converter 2 is set to constant voltage control, whilst converters 1 and 3 are in constant power mode. The time constant of the compensated outer power control loop is 10 times larger than the one of the compensated inner current control. The DC voltage control is tuned by means of a symmetrical optimum (phase margin 65°), with an overall DC system time constant of 22.3 ms, of which 5.4 ms results from each converter in the system. The rectified power in converter 2 is set to 662 MW, the inverted power in converters 1 and 3 is respectively equal to 150 MW and 500 MW.

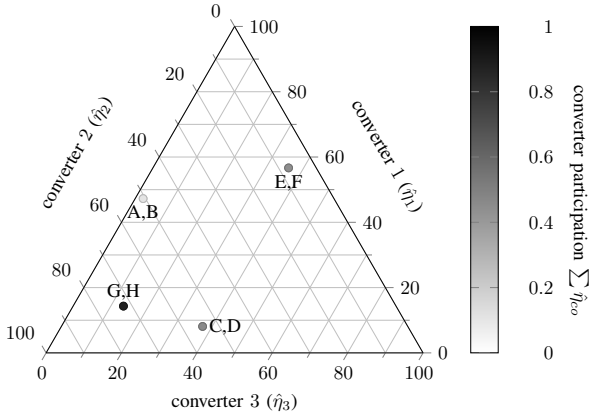

Figure 8. Converter participation in interaction modes – power control on converters 1 and 3, voltage control on converter 2.

Fig. 6a shows the eigenvalues of the entire system, limited to the ones with the real part over -1000. As a result, the plot is limited to 86 relevant modes out of a total of 112 modes. Fig. 6b depicts the eigenvalues related to converter 1 (i.e. $\eta_1 > 5\%$). Fig. 6c shows the cable modes (i.e. modes for which the sum of the cable participation $\eta_{1\text{-}2} + \eta_{2\text{-}3}$ is over

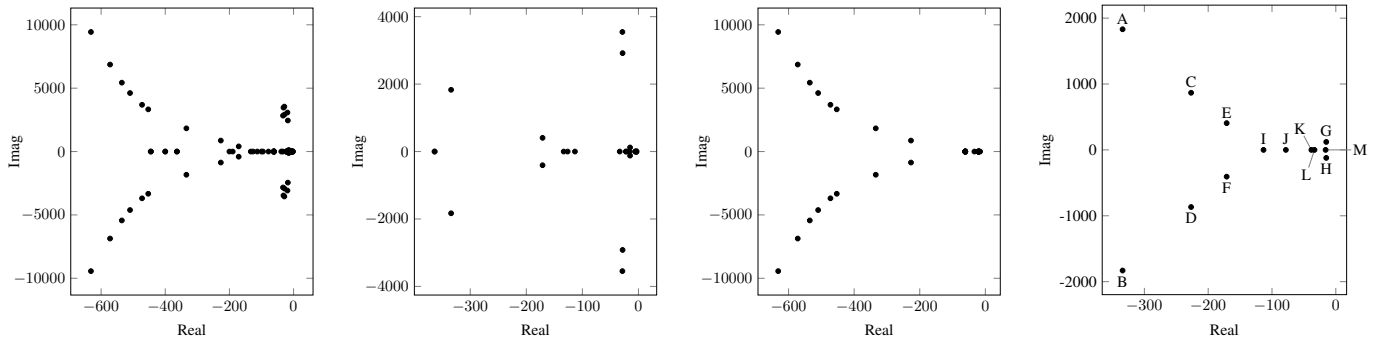

(a) Eigenvalues $\mathsf{A_t}$ (system) (b) Modes converter 1 ($\eta_1 > 5\%$) (c) Cable modes ($\eta_{1\text{-}2}+\eta_{2\text{-}3} > 50\%$) (d) Converter interaction modes ($\eta_{co} > 5\%$ for at least 2 converters)

Figure 9. Pole location of the system matrix $\mathsf{A_t}$, modes related to converter 1, cable modes, converter interaction modes – droop control on all converters.

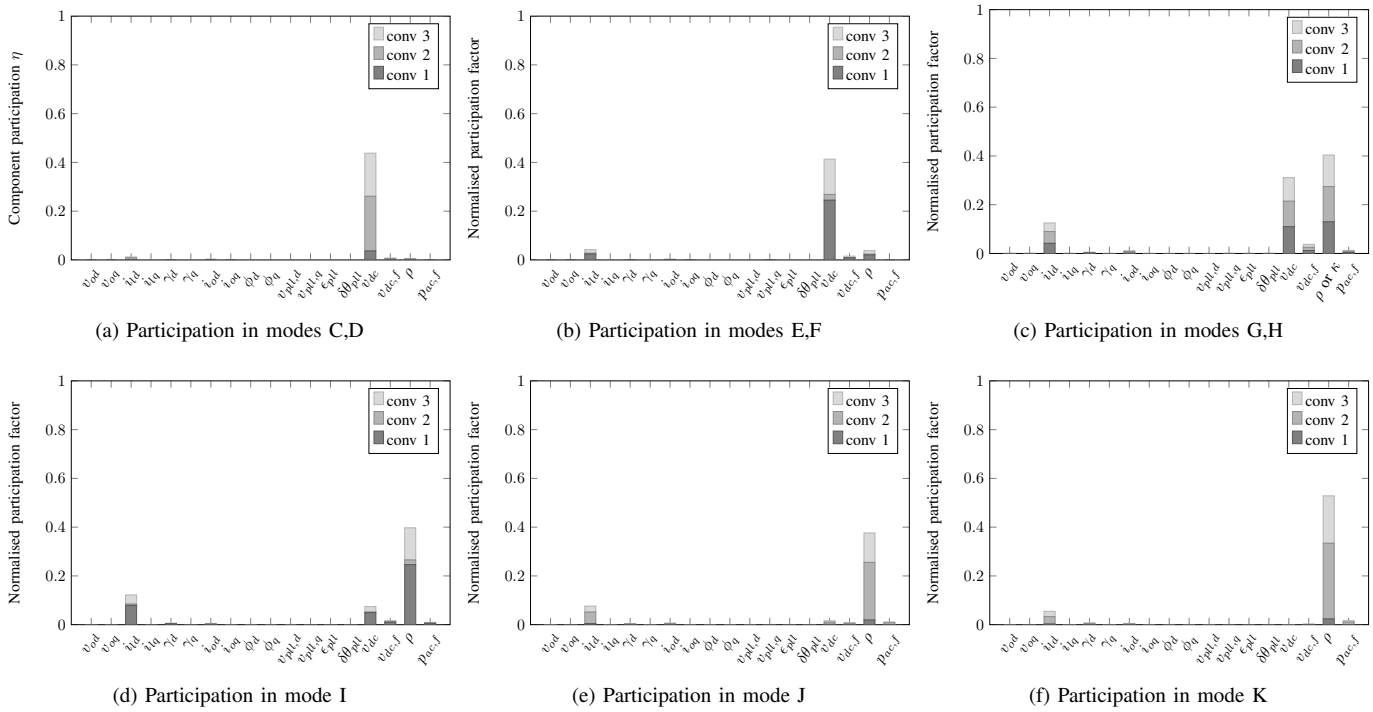

(a) Participation in modes C,D (b) Participation in modes E,F (c) Participation in modes G,H

(d) Participation in mode I (e) Participation in mode J (f) Participation in mode K

Figure 10. Participation in selected interaction modes – droop control.

50%). Fig. 6d shows the interaction modes between converters, i.e. the modes for which $\eta > 5\%$ for at least two converters. Only a limited subset of 8 out of 112 modes are identified as interaction modes between the converters based on the threshold for η of 5 %.

Fig. 7 shows the normalised values of the participation factors for a selection of interaction modes. These values are defined as $|p_{ki}|/\|\boldsymbol{p_i}\|$, with $\|\cdot\|$th L_1-norm. Modes A and B are not depicted, but can be shown to be mainly cable modes. It is clear from this picture that the main participating states in interaction modes C,D and E,F are the DC voltages v_{dc}. The main states participating in the slow modes G,H are the three voltages, which participate equally, as well as the state κ, which is related to the integrator of the DC voltage controller in converter 2 and to a lesser extent to the corresponding converter current component i_{ld}, associated with the active power. Fig. 8 shows the relative share of the different converters in the interaction modes A to H. The grayscale indicates the participation of the cables in the modes. It is clear that modes A,B are mainly associated with the cable modes, and that the slow modes G,H are mainly associated with the converters. The latter modes are strongly related to the power flow control in the system. It is clear from the above that the converter interactions in the DC system are not only limited to these slow control modes. Besides, the coupling is mostly associated with the DC voltage and associated states.

B. Voltage droop control

When using voltage droop control, the interaction pattern changes. This droop control has been modelled as a setpoint change of the active power reference for all converters, with the setpoint a function of the DC voltage. The droop gain has

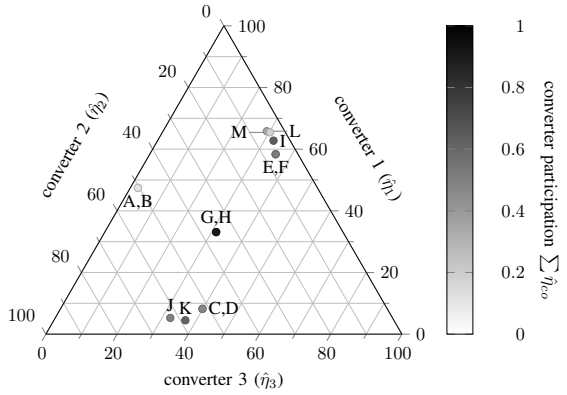

Figure 11. Converter participation in interaction modes – droop control.

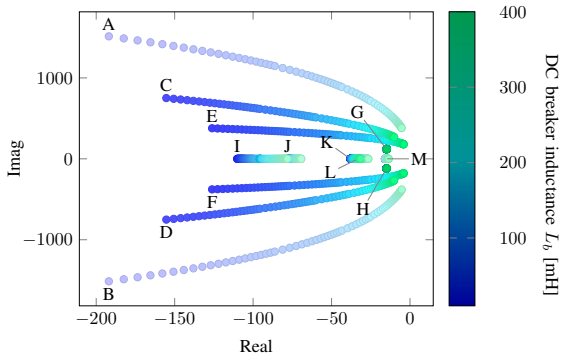

Figure 12. Interaction modes – variation of DC breaker inductance L_b.

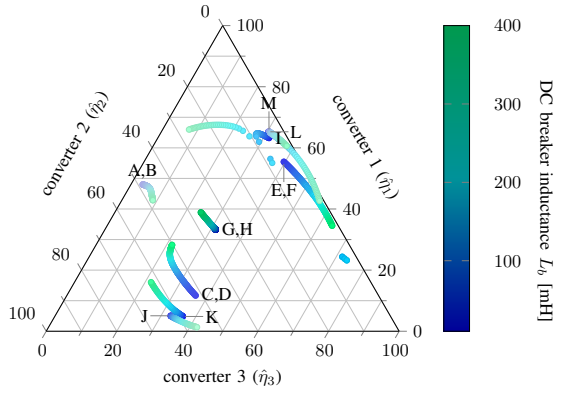

Figure 13. Converter participation in interaction modes – variation of DC breaker inductance L_b.

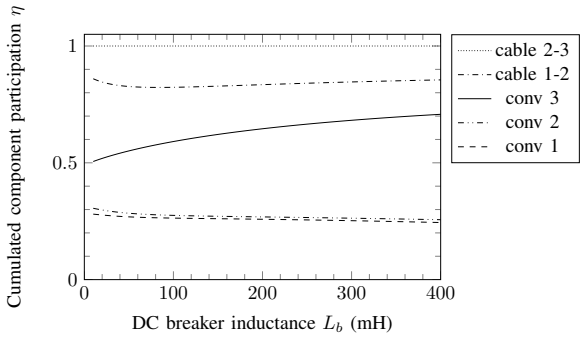

Figure 14. Participation modes E&F – variation of DC breaker inductance L_b.

been set to 0.1 for all converters. The active power of the converters is now equal to 327 MW, 1019 MW and 676 MW for respectively converters 1, 2 and 3. As in the previous section, Figs. 9–10 show the modes and the participation of the different converter state variables in a subset of interaction modes. The interaction modes A to F, which are associated with the cables remain largely unchanged when droop control is added. The interacting states in the slow control modes G,H now include the state variables ρ related to the integrator in all active power proportional integral (PI) controllers and the corresponding current components i_{ld} to a lesser extent. Furthermore, also other real poles appear in the interaction pattern. Fig. 10 shows the participation of the interacting states I to K as an example. These modes are most related to the state variable ρ associated with the integrating control action of power controller.

Fig. 11 depicts the relative participation of the different converters in the interaction modes. Comparison with Fig. 8 shows that the power interaction pattern of the interaction modes associated with the cables (A to F) does not change when the droop control is added. The different operating point does not affect the interaction pattern significantly. As a result of equal droop settings in all converters, the slow interaction mode G,H now faces equal participation from all converters, whereas it was primarily determined by the voltage controlling converter 2 in Fig. 8. The interaction modes J and K are close to the interaction (cable) modes C,D, indicating a similar relative participation of the converters. A similar remark holds for modes I, L and M on the one hand and modes E,F on the other hand. This was also visible from Fig. 10. When the voltage control is distributed by means of voltage droop control, the interactions between the converters are thus no longer limited to the DC voltage states, but also to related converter states.

V. Parametric Sensitivity of Interaction Modes

In this section, the effect of parameter variations to the location and relative participations of the interaction modes are analysed. The analysis has been limited to the case with voltage droop control on all converters.

A. Variation of DC breaker inductance

As a first example, inductors are added at the cable ends to represent the effect of DC breakers. Figs. 12–13 respectively illustrate the effect on the position of the poles in the complex plane and of the participation of the converters when changing their values from 10 mH to 400 mH. Similarly to the grayscale in previous ternary diagrams, the luminance of the colour indicates the cable participation in the mode. It is clear from Fig. 12 that adding the inductors largely leaves the position of interaction (power) modes G,H unaltered, while the cable modes A to F become much less damped and lower in frequency as a result of the increasing the inductance.

From Fig. 13, it can be observed that the participation of converter 1 slightly increases for modes G,H, mostly at the

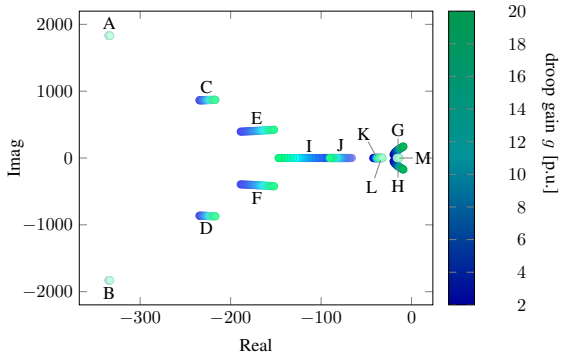

Figure 15. Interaction modes – variation of droop gain g in all converters.

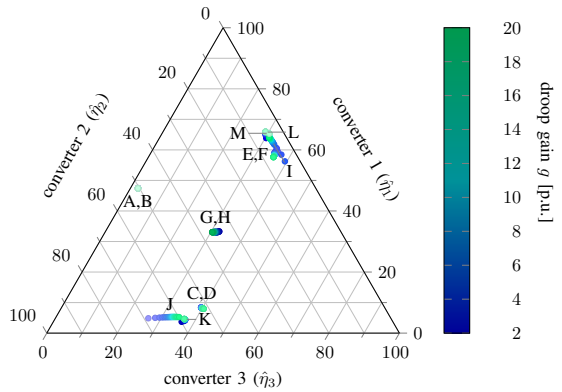

Figure 16. Converter participation in interaction modes – variation of droop gain g in all converters.

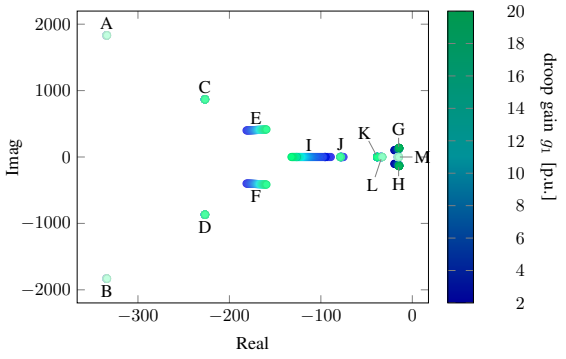

Figure 17. Interaction modes – variation of droop gain g in converter 1.

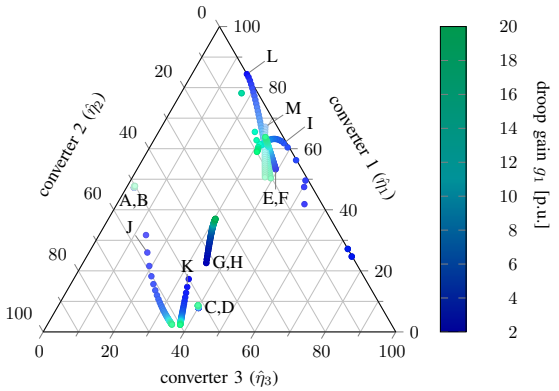

Figure 18. Converter participation in interaction modes – variation of droop gain g in converter 1.

expense of converter 3. Similarly, modes C,D and K face a similar, but more pronounced change in participation from the different converters. Whereas these interactions are initially primarily linked with the shorter cable between converters 2 and 3, they now present an increased share of converter 1, the remote converter, since the relative difference between the overall inductance of connections 1-2 and 2-3 decreases. Similarly, modes E,F, which are primarily linked to an interaction between converters 1 and 3, now face an increased share of converter 3 due to the relatively larger increased inductance of connection 2-3. Fig. 14 highlights how the increased share of converter 3 in the mode largely comes at the expense of the participation of cable 1-2.

B. Variation of all droop gains

Next, a variation of the droop gain g from 2 to 20 for all converters is considered. Figs. 15–16 summarise the results. Increasing the droop gain slightly changes the position of the cable modes C to F, whilst the relative participation of the converters largely remains unchanged. Mainly modes I and J, which are related to the integrating part of the power controller, face a change in the relative converter participation. The relative converter participation for the slow control modes G,H does not change significantly, but with increasing system gain, the corresponding frequency increases whilst the damping decreases.

C. Variation of droop gain in converter 1

As a last example, the droop gain in the remote converter 1 is varied, whilst the gain in converters 2 and 3 is kept equal to 10. Figs. 17–19 show the results. After comparison with the previous case, it is clear that changing only one droop gain has a greater effect on the relative converter participation in the interaction modes. For example, the relative participation of converter 1 in the slow mode G,H almost doubles. Modes E,F, which initially have a low participation from converter 1 (Fig. 10b), are not affected. Mode I, which had a relatively large share of converter 1 (Fig. 10d), is largely affected, both in position and component participation. The position of mode J remains largely unchanged, whilst the component participation changes for small values of g_1 (Fig. 19).

VI. Conclusions

The classification method presented in this paper allows to accurately distinguish between local converter modes and HVDC system interaction modes. Hereby, the method offers an extension of the widely adopted concept of local and interarea modes in AC systems. Moreover, this approach can assist in identifying possible sources of interactions between terminals and in designing corrective actions.

Numerical examples have been presented to highlight how this classification offers physical insights in the interaction patterns in HVDC systems. It is shown how interactions between converters are mainly associated with the DC voltages in the

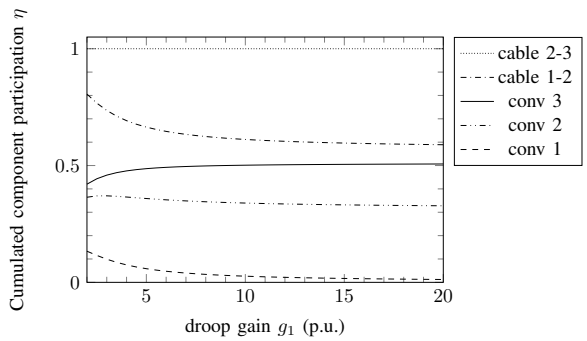

Figure 19. Participation mode J – variation of droop gain g_1 in converter 1.

system. When the voltage control is distributed throughout the system by employing droop control, the converter controllers become more coupled and other interactions appear related to associated control loops. Changing the droop gains modifies the participation of the converters in the interaction modes. Changing all converter droop gains largely affects the nature of the slower control modes, whilst leaving the participation of the different converters relatively unchanged. Only changing one converter droop gain at a time mainly changes the relative participation of the converters in the slow control mode. Including inductors to limit the rate of change of the currents has the largest effect on the cable modes, but leaves slower interaction modes largely unaffected.

APPENDIX

The appendix contains the state-space model of the cable from Fig. 3 and show how the state-space matrix A changes if inductors (from the DC breakers) are present at each cable end.

$$\boldsymbol{x} = \begin{bmatrix} i_{in} & v_0 & \boldsymbol{x_{cab}} & v_n & i_{out} \end{bmatrix}^T$$

$$\mathsf{A} = \begin{bmatrix} \frac{R_{b,in}}{L_{b,in}} & -\frac{1}{L_{b,in}} & & & \\ \frac{2}{C} & -\frac{G}{C} & -\frac{2}{C} \quad \cdots \quad -\frac{2}{C} & & \\ & \frac{1}{L_1} & & & \\ & \vdots & \mathsf{A}_{\mathsf{cab}} & -\frac{1}{L_1} & \\ & \frac{1}{L_N} & & \vdots & \\ & & & -\frac{1}{L_N} & \\ & & \frac{2}{C} \quad \cdots \quad \frac{2}{C} & -\frac{G}{C} & -\frac{2}{C} \\ & & & \frac{1}{L_{b,out}} & \frac{R_{b,out}}{L_{b,out}} \end{bmatrix}$$

$$\mathsf{B} = \begin{bmatrix} \frac{1}{L_{b,in}} & \\ & -\frac{1}{L_{b,out}} \end{bmatrix}^T$$

$$\boldsymbol{u} = \begin{bmatrix} v_{in} & v_{out} \end{bmatrix}^T$$

The state variables $\boldsymbol{x_{cab}}$ correspond to the internal current and voltage states of the cable model. The corresponding submatrix $\mathsf{A}_{\mathsf{cab}}$ refers to the state-space representation of the cable with parallel branches from [18], where variable v_{in} and v_{out} coincided with respectively state variables v_0 and v_n at the cable ends.

REFERENCES

[1] D. Van Hertem and M. Ghandhari, "Multi-terminal VSC HVDC for the European supergrid: Obstacles," *Renewable and Sustainable Energy Reviews*, vol. 14, no. 9, pp. 3156–3163, Dec. 2010.

[2] P. Kundur, *Power System Stability and Control*. McGraw-Hill Inc, New York, 1993.

[3] P. Kundur, J. Paserba, V. Ajjarapu, G. Andersson, A. Bose, C. Canizares, N. Hatziargyriou, D. Hill, A. Stankovic, C. Taylor, T. Van Cutsem, and V. Vittal, "Definition and classification of power system stability IEEE/CIGRE joint task force on stability terms and definitions," *IEEE Trans. Power Syst.*, vol. 19, no. 3, pp. 1387–1401, Aug. 2004.

[4] L. Harnefors, M. Bongiorno, and S. Lundberg, "Input-admittance calculation and shaping for controlled voltage-source converters," *IEEE Trans. Ind. Electron.*, vol. 54, no. 6, pp. 3323–3334, Dec. 2007.

[5] L. Zhang, L. Harnefors, and H.-P. Nee, "Modeling and control of VSC-HVDC links connected to island systems," *IEEE Trans. Power Syst.*, vol. 26, no. 2, pp. 783–793, 2011.

[6] L. Xu and L. Fan, "Impedance-based resonance analysis in a VSC-HVDC system," *IEEE Trans. Power Del.*, vol. 28, no. 4, pp. 2209–2216, Oct. 2013.

[7] J. Zhou, H. Ding, S. Fan, Y. Zhang, and A. Gole, "Impact of short-circuit ratio and phase-locked-loop parameters on the small-signal behavior of a VSC-HVDC converter," *IEEE Trans. Power Del.*, vol. 29, no. 5, pp. 2287–2296, Oct. 2014.

[8] E. Prieto-Araujo, F. D. Bianchi, A. Junyent-Ferre, and O. Gomis-Bellmunt, "Methodology for droop control dynamic analysis of multiterminal VSC-HVDC grids for offshore wind farms," *IEEE Trans. Power Del.*, vol. 26, no. 4, pp. 2476–2485, 2011.

[9] G. O. Kalcon, G. P. Adam, O. Anaya-Lara, S. Lo, and K. Uhlen, "Small-signal stability analysis of multi-terminal VSC-based DC transmission systems," *IEEE Trans. Power Syst.*, vol. 27, no. 4, pp. 1818–1830, Nov. 2012.

[10] R. Preece and J. Milanovic, "Tuning of a damping controller for multi-terminal VSC-HVDC grids using the probabilistic collocation method," *IEEE Trans. Power Del.*, vol. 29, no. 1, pp. 318–326, Feb. 2014.

[11] G. Pinares, L. Tjernberg, L. A. Tuan, C. Breitholtz, and A.-A. Edris, "On the analysis of the dc dynamics of multi-terminal VSC-HVDC systems using small signal modeling," in *Proc. IEEE PowerTech 2013*, Grenoble, France, Jun., 16–20 2013, 6 pages.

[12] N. Chaudhuri, R. Majumder, B. Chaudhuri, and J. Pan, "Stability analysis of VSC MTDC grids connected to multimachine AC systems," *IEEE Trans. Power Del.*, vol. 26, no. 4, pp. 2774–2784, Oct. 2011.

[13] W. Wang, A. Beddard, M. Barnes, and O. Marjanovic, "Analysis of active power control for VSC-HVDC," *IEEE Trans. Power Del.*, vol. 29, no. 4, pp. 1978–1988, Aug. 2014.

[14] P. Rault, "Dynamic modeling and control of multi-terminal HVDC grids," Ph.D. dissertation, Ecole Centrale de Lille, Mar. 2014.

[15] M. Parniani and M. Iravani, "Computer analysis of small-signal stability of power systems including network dynamics," *IEE Proc.-Gener. Transm. Distrib.*, vol. 142, no. 6, pp. 613–617, Nov. 1995.

[16] N. Pogaku, M. Prodanovic, and T. Green, "Modeling, analysis and testing of autonomous operation of an inverter-based microgrid," *IEEE Trans. Power Electron.*, vol. 22, no. 2, pp. 613–625, Mar. 2007.

[17] S. D'Arco, J. A. Suul, and M. Molinas, "Implementation and analysis of a control scheme for damping of oscillations in VSC-based HVDC grids," in *Proc. PEMC 2014*, Antalya, Turkey, Sep., 21-24 2014, 8 pages.

[18] J. Beerten, S. D'Arco, and J. A. Suul, "Cable model order reduction for HVDC systems interoperability analysis," in *Proc. IET ACDC 2015*, Birmingham, UK, Feb., 10-12 2015, 10 pages, accepted for publication.

[19] B. Gustavsen and A. Semlyen, "Rational approximation of frequency domain responses by vector fitting," *IEEE Trans. Power Del.*, vol. 14, no. 3, pp. 1052–1061, Jul. 1999.

[20] W. Leterme, N. Ahmed, J. Beerten, L. Ängquist, D. Van Hertem, and S. Norrga, "A new HVDC grid test system for HVDC grid dynamics and protection studies in EMT-type software," in *Proc. IET ACDC 2015*, Birmingham, UK, Feb., 10-12 2015, 7 pages, accepted for publication.

[21] J. Beerten, S. Cole, and R. Belmans, "Generalized steady-state VSC MTDC model for sequential AC/DC power flow algorithms," *IEEE Trans. Power Syst.*, vol. 27, no. 2, pp. 821–829, May 2012.